Solar Energy 165 (2018) 75–84

Contents lists available at ScienceDirect

Solar Energy

journal homepage: www.elsevier.com/locate/solener

Design and modeling of a spectrum-splitting hybrid CSP-CPV parabolic trough using two-stage high concentration optics and dual junction InGaP/GaAs solar cells

Bennett Widyolar[a,b], Lun Jiang[a,b,*], Mahmoud Abdelhamid[a,b], Roland Winston[a,b]

[a] University of California, Merced – 5200 Lake Rd, Merced, CA 95343, USA
[b] University of California, Advanced Solar Energy Institute (UC Solar), USA

ARTICLE INFO

Keywords:
Spectral beam splitting
Hybrid solar CSP/CPV
Compound parabolic concentrator
Nonimaging optics

ABSTRACT

A novel hybrid concentrating solar power/concentrating photovoltaic (CSP/CPV) collector is designed, simulated, and optimized for the purpose of power generation. The two-stage concentrator combines a primary parabolic trough with a secondary compound parabolic concentrator (CPC). Single junction Indium Gallium Phosphide (InGaP) and dual junction (InGaP)/Gallium Arsenide (GaAs) solar cells are examined as spectrally reflective beam splitting solar cells. The secondary CPC profile is optimized to guarantee geometric efficiency despite a non-continuous (i.e. segmented) profile and the final two-stage design achieves a geometric concentration ratio of 50× on the thermal absorber. Optical, thermal, and cell performance models are used to determine net electric production for different configurations of the hybrid collector and combined with cost estimates to calculate $\$/W_{exergy}$ and $\$/W_{electric}$. The down-selected design incorporates dual junction InGaP/GaAs cells, achieves 40% solar-to-exergy efficiency and 23% solar-to electric-efficiency at 600 °C, with a thermal fraction of 73% and installs for an estimated $\$2.15/W_{electric}$.

1. Introduction

In the application of solar to electric power generation there are two main techniques: *Concentrating Solar Power* (CSP) and *Photovoltaics* (PV).

CSP systems generate electricity in a similar fashion to typical power plants, but using concentrated solar radiation to generate useful temperatures in a heat transfer fluid (HTF) which is delivered to a steam Rankin cycle. Most CSP plants use parabolic troughs (Fernández-García et al., 2010) operating with thermal oils near 400 °C and achieve instantaneous solar to electric conversion efficiencies around 20% (Price et al., 2002). The conversion of heat to work in CSP plants is limited by the maximum Carnot efficiency (η_{Carnot}), described by equation 1, which increases with the temperature difference between the hot (T_H) and cold (T_C) reservoirs.

$$\eta_{Carnot} = 1 - \frac{T_C}{T_H} \tag{1}$$

As a result, the main drive in CSP research today is toward the development of high concentration systems (power towers with concentration ratios > 1000) (Behar et al., 2013) capable of generating temperatures > 700 °C and both high temperature receivers and HTFs (Vignarooban et al., 2015) (molten salts, solid particulates, gases) which can operate efficiently and reliably at such temperatures (Mehos et al., 2017).

PV systems generate electricity by an entirely different, wavelength-dependent quantum process. A PV semiconductor is responsive at a single wavelength, dictated by its material bandgap energy. Photons with energies above the bandgap generate electron hole pairs and produce a usable current. Low energy photons are absorbed as heat and the excess energy in high energy photons is converted to heat through a process known as thermalization. Thus, with a low energy cutoff and diminishing returns at higher energies, solar cells are most effective at generating electricity within specific spectral windows which limits single-junction cells to a maximum ~33.5% solar to electric efficiency (Shockley and Queisser, 1961). This is most closely approached by Gallium Arsenide (GaAs) which has demonstrated a small area cell efficiency of 28.8% (Green, 2017), but commonly available commercial silicon *modules* are closer to ~20% (Smith et al., 2013).

Multi-junction cells under concentration, however, have achieved efficiencies up to 46% (Green et al., 2017). This is made possible by stacking cells with different bandgaps to optimally harvest separate portions of the solar spectrum as it is transmitted through the stack. This technique is known as spectral beam splitting (SBS), where the

* Corresponding author at: University of California, Merced – 5200 Lake Rd, Merced, CA 95343, USA.
E-mail addresses: bwidyolar@ucmerced.edu (B. Widyolar), ljiang2@ucmerced.edu (L. Jiang), mabdelhamid@ucmerced.edu (M. Abdelhamid), rwinston@ucmerced.edu (R. Winston).

https://doi.org/10.1016/j.solener.2018.03.015
Received 16 August 2017; Received in revised form 1 March 2018; Accepted 5 March 2018
Available online 20 March 2018
0038-092X/

Nomenclature

η_{Carnot}	carnot efficiency
T_c	cold reservoir temperature
T_H	hot reservoir temperature
C,C_x	concentration ratio
θ	half acceptance angle
ϕ	half rim angle
f	focal length
A_1	primary aperture area
A_2	secondary aperture area
A_3	absorber area
η_{cell}	cell efficiency
q	elementary charge
λ	wavelength
h	Planck's constant
c	speed of light
EQE	external quantum efficiency
V_{oc}	open circuit voltage
FF	fill factor
η_{band}	in-band cell efficiency
G_{direct}	ASTM direct reference spectrum
ρ	reflectance
τ	transmittance
α	absorptance
β	temperature coefficient
$C_{x,strip}$	concentration on strip
A_{strip}	area of cell strip
$\eta_{0,strip}$	incident light on strip
$\eta_{cell,strip}$	efficiency of cell strip
η_{Cx}	efficiency boost from concentration
n_{strips}	number of strips
$\eta_{system,cells}$	system cell efficiency
$\eta_{cell,cooling}$	waste heat efficiency
$\eta_{abs,strip}$	amount absorbed by cell strip
ϵ	emissivity
$\eta_{thermal}$	thermal efficiency
$\eta_{0,thermal}$	optical efficiency of thermal stream
σ	Stefan-Boltzmann constant
T_{abs}	absorber temperature
T_∞	ambient temperature
DNI	direct normal irradiance
η_{exergy}	exergy efficiency
η_{HX}	plant thermal efficiency
$\eta_{PB,net}$	power block net efficiency
$\eta_{electric}$	solar-to-electric conversion efficiency

Abbreviations

CSP	concentrating solar power
PV	photovoltaics
HTF	heat transfer fluid
GaAs	gallium arsenide
SBS	spectral beam splitting
TES	thermal energy storage
CPV	concentrating photovoltaics
PTC	parabolic trough collector
HCE	heat collecting element
CPC	compound parabolic concentrator
CAP	concentration acceptance product
InGaP	indium gallium phosphide
ASTM	American Society of Testing Materials
SAM	system advisor model

solar spectrum is harnessed as a tool to maximize conversion efficiency.

In the past 5 years the price of installed solar PV in the US has dropped by a factor of two (Fu et al., 2016), increasing solar penetration onto the grid and manifesting effects such as the "Duck Curve" in California which has reduced grid stability and the value of additional PV installations (Palmintier et al., 2016). Time-shifted energy production is possible through the deployment of battery banks, but current costs are large enough to not be economically viable. Thermal energy storage (TES), on the other hand, is a relatively cheap addition to a CSP plant which enables *dispatchable* renewable electricity generation (Mehos et al., 2016) and increases the value of additional capacity on the grid (Denholm et al., 2013). Deployment of these systems on a meaningful scale, however, requires reductions to the currently high capital costs for CSP systems.

In 2013, ARPA-E released the FOCUS solicitation (Advanced Research Projects Agency, 2014) to develop advanced hybrid solar converters which, by employing SBS, could more optimally exploit the solar spectrum and reach higher conversion efficiencies. In doing so they might be able to reduce the levelized electricity cost from hybrid plants to a point where these plants are economically viable and enable deployment of TES systems (Branz et al., 2015). The program has revitalized the field with an emphasis on experimental work, which to-date has been sparse compared to the published theoretical works. For a detailed summary on the historical and current state of SBS research, the reader is referred to the following review papers by Imenes and Mills, 2004, Mojiri et al., 2013, Ju et al., 2017.

To date much of the research has been performed in China, Australia, and the U.S. (Ju et al., 2017). Most SBS systems use either interference filters (Orosz et al., 2016; Yu et al., 2015; Raush and Chambers, 2014) or liquid absorptive filters (Otanicar et al., 2016; DeJarnette et al., 2016; DeJarnette et al., 2015) to perform spectrum splitting, which are tuned to match the solar cells being used. Silicon cells are by far the most common solar cells studied due to their low cost and availability, but the qualities that make them ideal as one-sun cells (low, broad-band conversion efficiency) makes them less so for spectrum splitting systems (Widyolar et al., 2018) and III–V cells and multi-junction cells are becoming more common. Linear Fresnel (Liu et al., 2014), parabolic trough (Stanley et al., 2016), dish (Shou et al., 2011; Xu et al., 2016), and tower configurations (Segal et al., 2004) have all been described with typical design solar-to-electric efficiencies between 20 and 30%. The economics of trough systems (drop-in retrofit and new) has been calculated between \$1.0 and 2.30/$W_{electric}$ (Duquette and Otanicar, 2012; Orosz et al., 2016).

Remaining challenges for interference filters include cost reduction for large filters and angular spectral control, whereas absorptive filter systems require further development with regards to stability and high temperature operation. Beam splitting also tends to reduce operating temperatures which limits the ability to charge thermal storage systems and brings into question its practical application. With so many different techniques, applications, and preferred metrics, it becomes difficult to compare between systems reported in the literature. The most recent review (Ju et al., 2017) highlighted these issues, indicating the need for higher temperature designs, standardized metrics, and a better understanding of the economics of hybrid SBS systems.

In this paper we develop and optimize a CSP/CPV receiver for power generation which employs a novel spectrum splitting technique using *spectrally selective solar cell mirrors*. A secondary nonimaging concentrator evens the flux distribution on the absorber and provides high concentration for efficient operation at elevated temperatures (> 600 °C). The use of solar cell mirrors bypasses issues with interference or absorptive filters. In Section 2 we design the optical system which is optimized to produce high concentration on the absorber and

incorporate flat solar cell strips into the secondary profile. In Section 3 we describe the various equations used to model performance of the different subsystems and the economic estimates used to generate the results presented in Section 4 for down-selection. The final design is to be developed into an experimental prototype and reported in subsequent publications.

2. Two-stage concentrator design and optimization

2.1. Two-stage optical design

The geometric concentration of typical parabolic trough systems with cylindrical absorbers is given by Eq. (2), where φ is the half-rim angle and θ the half-acceptance angle.

$$C_{PTC} = \frac{\sin\phi}{\pi\sin\theta} \tag{2}$$

Parabolic systems are designed with φ close to 90° to maximize their concentration, in which case equation 2 reduces to $(\pi\cdot\sin\theta)^{-1}$ and the concentration ratio is roughly 30X for a half-acceptance angle $\theta = 0.6°$ (Fernández-García et al., 2010). The thermodynamic limit for concentration in a 2D system with a faraway source (Winston, 1970), however, is given by Eq. (3) and therefore it should be possible to increase the concentration ratio by a factor of π.

$$C_{max} = \frac{1}{\sin\theta} \tag{3}$$

One approach is to use a secondary concentrator for which the concentration ratio of a two-stage system with an ideal secondary is described geometrically by Eq. (4) (Collares-Pereira et al., 1991).

$$C_{two-stage\ PTC} = \frac{\cos\phi}{\theta} \tag{4}$$

Concentration maximizes for small half rim angles, but anything less than 45° becomes somewhat less practical due to the long focal lengths they generate.

The proposed optical system uses the two-stage concentrator shown in Fig. 1. The primary concentrator is a 5 m wide 45° half-rim angle parabola which reflects light into a 45° half-angle beam on the secondary heat collecting element (HCE) at a focal distance (*f*) of 3.02 m. The secondary aperture area (A_2) is given by Eq. (5), where A_1 is the primary concentrator aperture width.

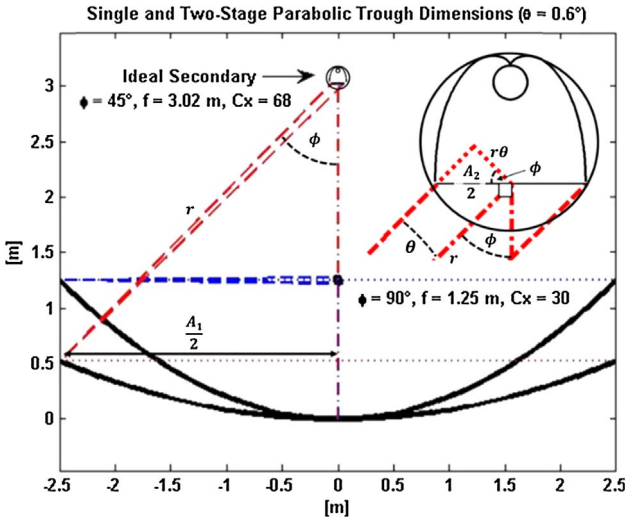

Fig. 2. Proposed two stage parabolic trough collector (PTC) design (red) overlaying typical single-stage PTC design (blue) with listed half-rim angles (ϕ), focal length (f), and concentration ratio (C_x). Both designs are for 5-m wide apertures and collectors with half-acceptance angle $\theta = 0.6°$.

$$A_2 = \frac{A_1\theta}{\sin\phi\cos\phi} \tag{5}$$

The secondary accepts light reflected by the primary and further concentrates it onto the thermal absorber (A_3). A half-acceptance angle $\theta = 0.6°$ yields a secondary aperture width of 105 mm and allows the secondary reflector and thermal absorber to fit inside a standard 120 mm glass tube. The acceptance angle accommodates the sun disk angle and other optical inaccuracies in the system such as mirror imperfections, structural bending, and optical misalignment. At solar noon, the 0.25° sun half-disk angle allows for a significant amount of optical tolerance in the system. As the sun moves off solar noon the skew angle makes the sun appear dilated and at ± 4 h from solar noon (± 60° skew angle) the sun has a half-disk angle of ~0.5° (Bendt et al., 1979; Cooper et al., 2016). For a half-acceptance angle of 0.6° the geometric concentration ratio approaches 68× (Schmitz et al., 2015) which is 71% of the ideal concentration ratio.

The geometry of the proposed two stage parabolic concentrator is plotted against a typical parabolic trough collector system in Fig. 2.

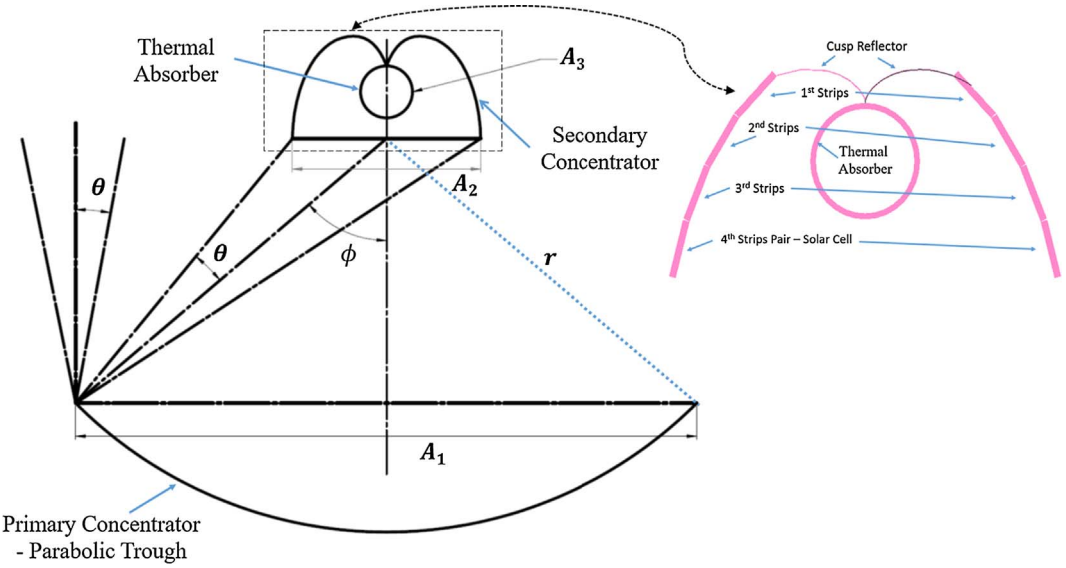

Fig. 1. Two-stage hybrid CSP/CPV design for an ideal secondary which is developed later in this paper to accommodate the profile with flat strips drawn in pink.

2.2. Secondary optimization

Sections of the CPC are to be replaced with high efficiency back-reflecting solar cells (see Fig. 1) which generate electricity from sub-bandgap photons and reflect remaining photons to the thermal absorber. Ray trace simulations generated the intensity profile along the CPC reflector in Fig. 3. A high intensity band located 10 mm from the center of the CPC and extending approximately 50 mm represents the ideal location for the cell placement.

Since the cells are not flexible, portions of the CPC profile must be approximated by flat segments. Ray tracing on a CPC approximated by 4 strips of 16 mm wide flat segments, however, reduced the geometric efficiency to 90%. To recover this loss a new design was developed (Widyolar et al., 2017) to guarantee edge ray incidence on the absorber (see Fig. 4). In doing the geometric efficiency was fully recovered, but at the expense of a 13% reduction in aperture area (concentration ratio). To maintain the required secondary aperture, the entire secondary design was scaled up to a final secondary aperture width of 110 mm and an absorber outer diameter of 32 mm. After these changes the system has a final geometric concentration ratio of $Cx = \frac{5000\text{ mm}}{\pi * 32\text{ mm}} = 50$, approximately 52% the theoretical limit.

The final parameters of the two-stage optical system are listed in Table 1. The full system (primary parabolic mirror and optimized CPC from Fig. 4) was modelled for an input angular spread of 0.25° and an incidence angle which was swept from 0° to 1°. Simulation results are presented in Fig. 5 which verifies the 0.6° acceptance angle.

2.3. Beam splitting potential

The desired properties of a solar cell for use in a beam splitting device are both (a) high conversion efficiency and (b) narrow band response. After screening various solar cells types, single junction Indium Gallium Phosphide (InGaP) and dual junction Gallium Arsenide (GaAs)/InGaP were selected as candidates and the external quantum efficiency (EQE), open circuit voltage (V_{oc}), and fill factors (FF) (Green et al., 2017) were used to calculate the spectral efficiency $\eta_{cell}(\lambda)$ according Eq. (5). Here q is the elementary charge in coulumbs, h is the Planck constant, c is the speed of light, and λ is the wavelength of light.

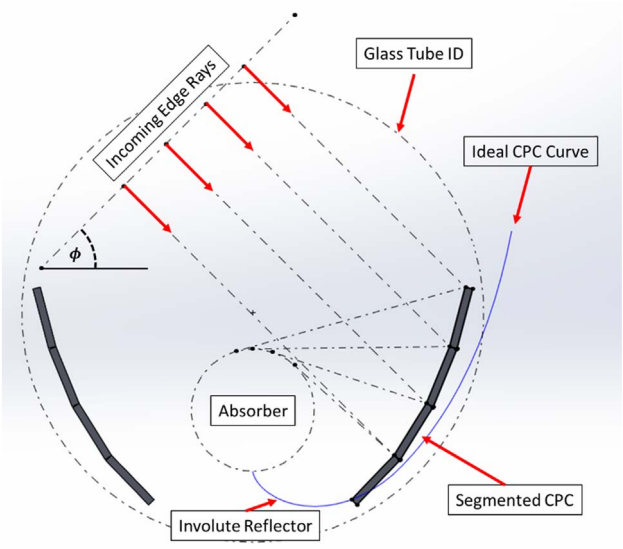

Fig. 4. Optimized secondary CPC shape where portions of profile are approximated by flat segments. The optimized profile has 100% geometric efficiency despite its non-ideal shape which is achieved at the expense of geometric concentration (Widyolar et al., 2017).

$$\eta_{cell}(\lambda) = q\frac{\lambda}{hc}EQE(\lambda)V_{oc}FF \tag{6}$$

The spectral efficiency of InGaP (dashed blue) and GaAs (dashed red) are plotted against the direct-beam solar spectrum in Fig. 6. The in-band efficiency (η_{band}) calculated according to Eq. (6) is the solar cell's effective efficiency within the spectral window bound by λ_1 and λ_2. These are also shown in for each cell above the x-axis in Fig. 6.

$$\eta_{band} = \frac{\int_{\lambda_1}^{\lambda_2}\eta_{cell}(\lambda)G_{direct}(\lambda)}{\int_{\lambda_1}^{\lambda_2}G_{direct}(\lambda)} \tag{7}$$

The Carnot efficiency (η_{Carnot}) is the thermodynamic limit for converting thermal energy into useful work calculated and is calculated

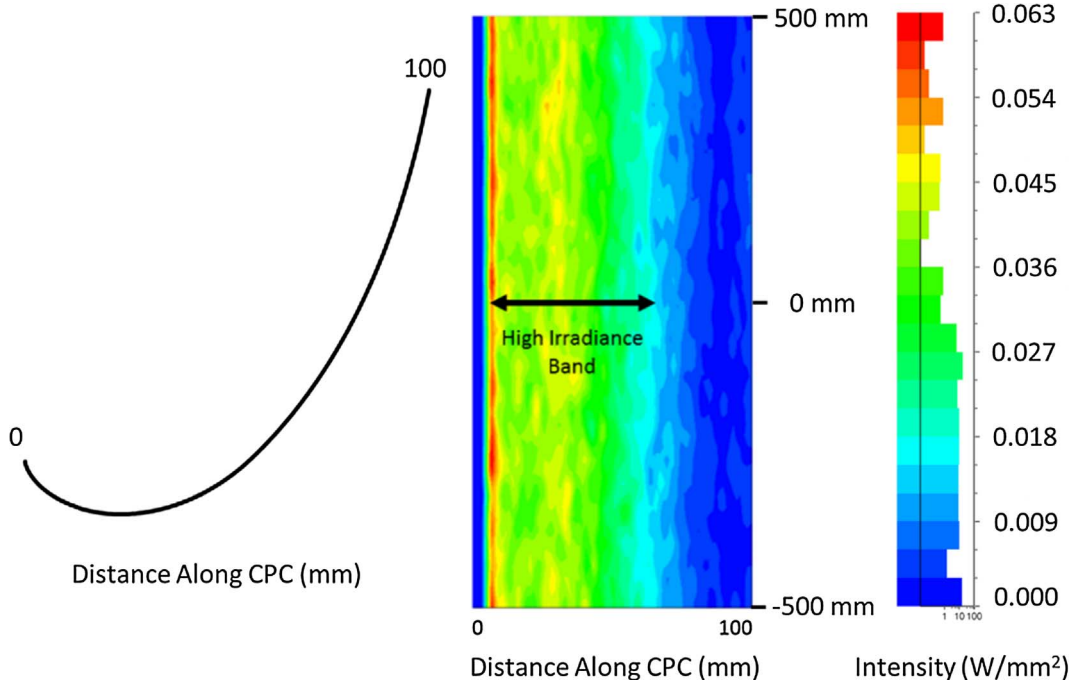

Fig. 3. Local light intensity on ideal secondary CPC reflector as reflected from 45° primary parabolic trough. The high irradiance band begins roughly 10 mm from the center of the CPC and extends roughly 50 mm.

Table 1
Two-stage concentrator parameters.

Design parameter	Value
ϕ	45°
θ	0.6°
A_1	5 m
A_2	110 mm
A_3	100 mm
C_1	45×
C_2	1.1×
C_{total}	50×
CAP^*	0.52

* Concentration Acceptance Product = $Csin\theta = C/C_{max}$. Relates how close the current system design is to the maximum theoretical concentration ratio.

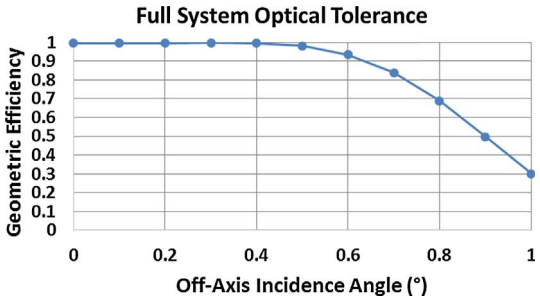

Fig. 5. Geometric efficiency on thermal absorber using optimized CPC from Fig. 4.

using Eq. (1), where T_H is the hot reservoir temperature and T_C is the cold reservoir temperature. Real engines typically only reach 2/3 of this thermodynamic limit and this is plotted in Fig. 6 (dashed red) for a target operating temperature (T_H) of 600 °C and cold reservoir temperature (T_C) of 37 °C, and listed as η_{band} for the thermal junction in Fig. 6. Also listed below the x-axis are the fractions of the direct beam solar spectrum within each spectral region from 0 to 670 nm, 670 to 875 nm, and 875 to 2500 nm.

The in-band efficiency of each junction multiplied by the fraction of the solar spectrum in each band yields a total solar-to-electric conversion efficiency of 49.1%. This is higher than what is achieved by any of the subsystems under full spectrum alone. While optical, thermal, and conversion losses will reduce this number in practice, this demonstrates the potential of beam splitting systems to achieve higher conversion efficiencies through optimal utilization of the solar spectrum.

3. Performance models

3.1. Optical model

Full optical simulations were performed using 1 million rays with the ASTM direct-beam solar spectrum as the input to the collector system. Shading from the 110 mm wide secondary aperture results in a 2.2% loss from the primary aperture. The parabolic mirror has a standard glass-silver mirror reflectance (ρ) of 0.92. The secondary concentrator, absorber, and solar cells are encased in a glass tube which is evacuated to 10^{-4} mbar to eliminate convective heat loss and isolate the hot absorber surface from the cells in close proximity. The glass has a transmittance (τ) of 0.95 after the assumed application of anti-reflective coatings to each surface. Characteristic spectral reflectance curves for a single junction InGaP and a dual junction InGaP/GaAs cell were measured using a spectrophotometer. The resulting curves (Figs. 7 and 8) are incorporated into the optical model to determine the amount of light reflected or absorbed by the cells. The remaining portion of the CPC profile which is not made from solar cells is assumed to be a polished aluminum mirror with a reflectance (ρ) of 95%. The solar-weighted absorptance (α) of the selective coating on the absorber is assumed to be 95%.

Optical performance is simulated for a thermal only receiver (no cells) and for a hybrid PV/T receiver with varying (4–8) numbers of solar cell strips. Simulations are performed for both single (InGaP) and dual junction (InGaP/GaAs) cells, with the cells always placed on the

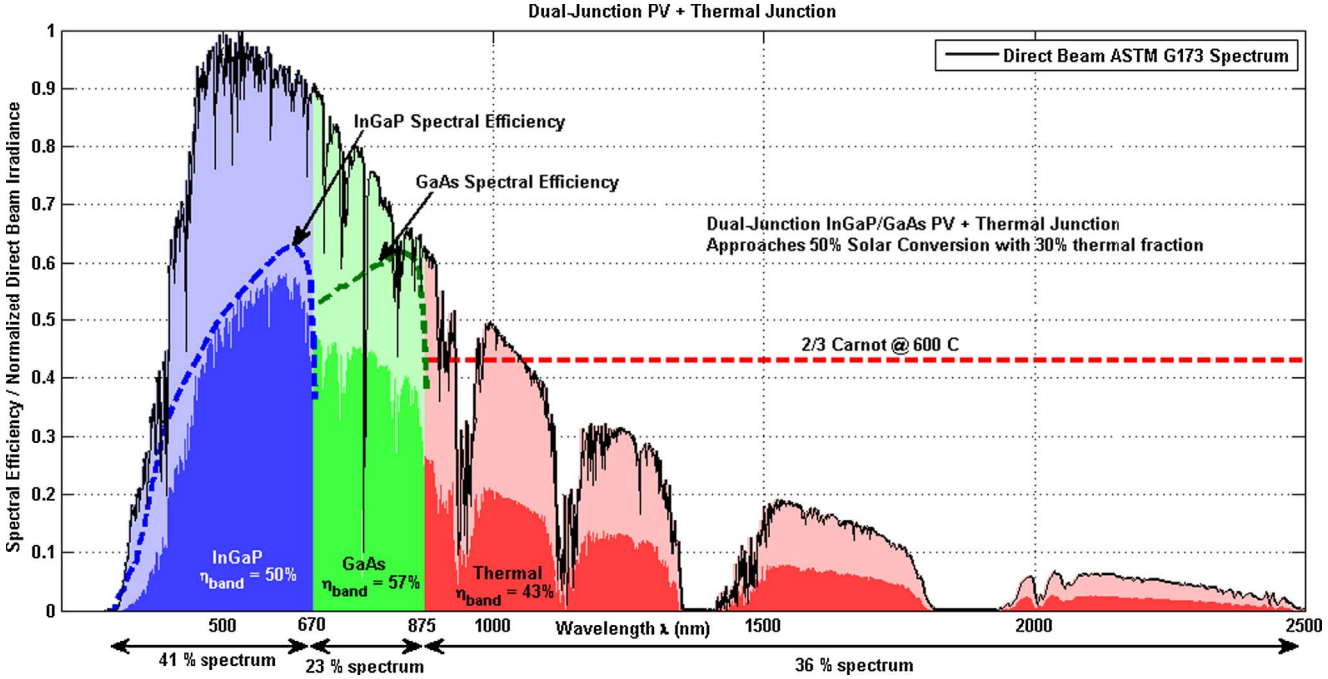

Fig. 6. Spectral beam splitting with dual junction PV and third thermal junction. InGaP and GaAs spectral efficiency curves (dashed blue and green) are adapted from the solar cell efficiency tables. The in-band efficiencies (η_{band}) are calculated according to Eq. (6) for the solar cells and assuming 2/3 Carnot efficiency (Eq. (1)) for the thermal junction. The fraction of the solar spectrum within each band is listed below the graph. Adding all of these together yields a solar-to-electric conversion efficiency which approaches 50% with a thermal fraction of 30%.

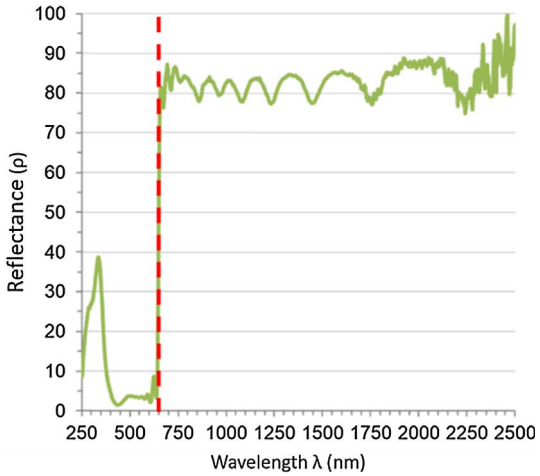

Fig. 7. Measured InGaP cell reflectance with bandgap at 670 nm shown by dashed line.

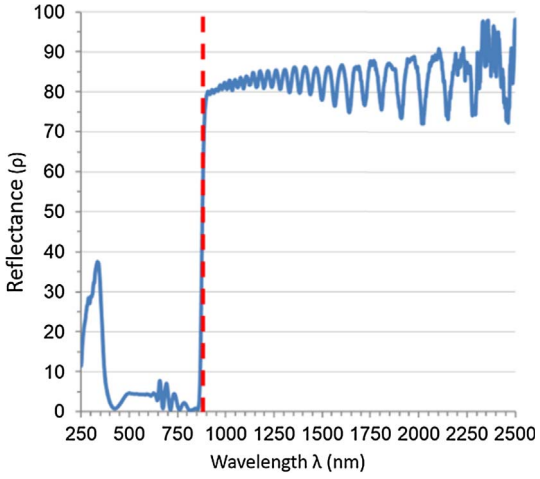

Fig. 8. Measured InGaP/GaAs cell reflectance with bandgap at 875 nm shown by dashed line.

Table 2
Optical simulation parameters.

Parameter	Value
$\rho_{primary}$	0.92
τ_{glass}	0.95
$\rho_{secondary}$	0.95
$\alpha_{absorber}$	0.95

Table 3
Solar cell properties.

	η_{cell} (%), 25 °C	β (%/°C)
InGaP Solar Cell	0.14	0.0002
InGaP/GaAs Solar Cell	0.23	0.0005

closest available strip to the absorber where they experience the highest flux (see Fig. 1).

The optical simulations generate several key parameters which are used later as inputs to the solar cell and thermal performance models: light absorbed by the high temperature absorber ($\eta_{0,thermal}$) and the light incident upon ($\eta_{0,strip}$) and absorbed ($\eta_{abs,strip}$) by each cell strip. Relevant optical parameters from the model are summarized in Table 2.

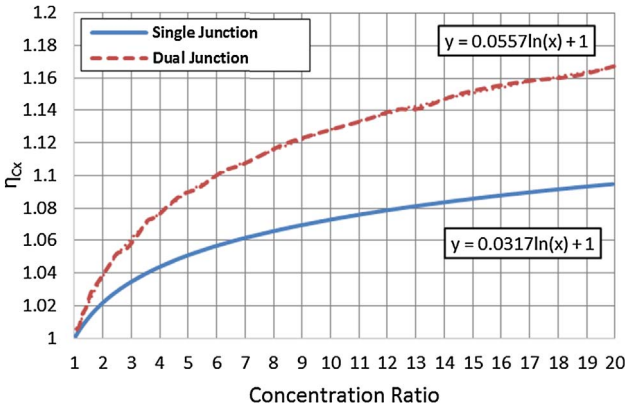

Fig. 9. Improvement in cell efficiency due to increased concentration with the single junction InGaP cell drawn solid blue and dual junction InGaP/GaAs cell drawn dashed red. (For interpretation of the references to color in this figure legend, the reader is referred to the web version of this article.)

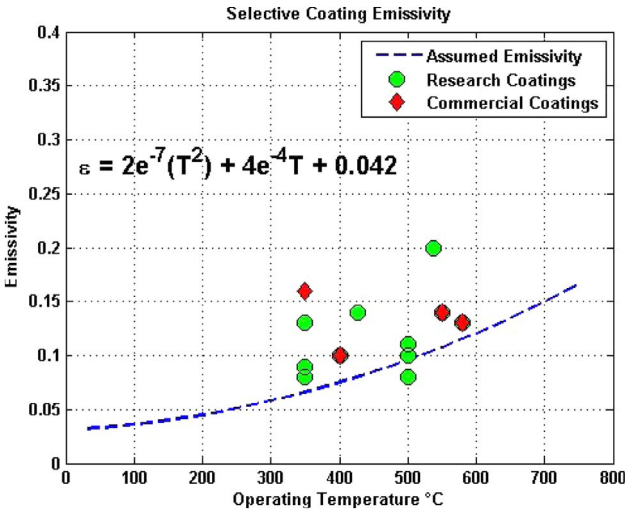

Fig. 10. The assumed emissivity profile of the selective coating used in this model plotted (dashed blue) against some selected commercial (red diamond) and research (green circle) coatings reported in Selvakumar and Barshilia (2012). (For interpretation of the references to color in this figure legend, the reader is referred to the web version of this article.)

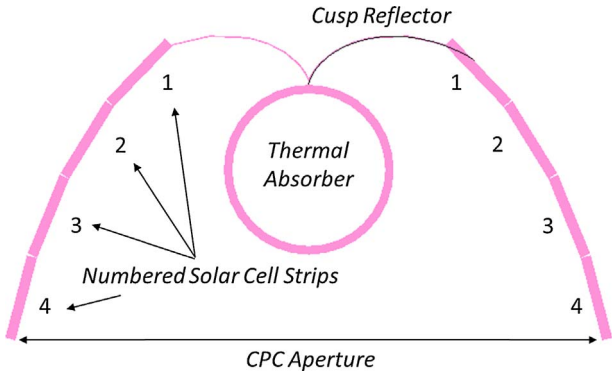

Fig. 11. Hybrid HCE schematic with numbered solar cell strips.

3.2. Solar cell model

The solar cells are modelled using the properties listed in Table 3. Cell efficiency is calculated as a function of concentration at an operating temperature of 40 °C.

The solar concentration on each strip $C_{x,strip}$ is estimated from

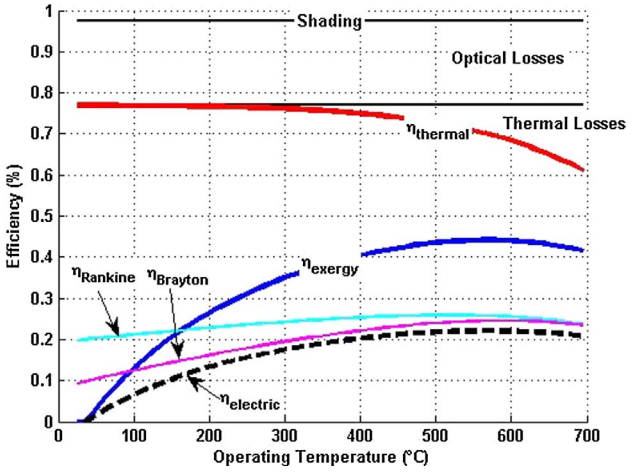

Fig. 12. Simulated performance of thermal-only collector.

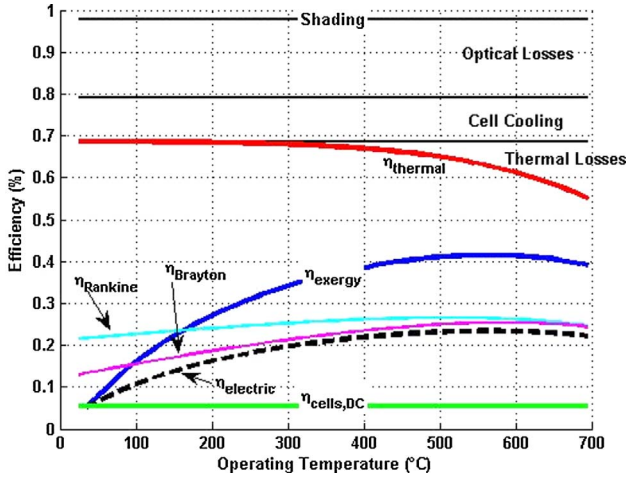

Fig. 13. Simulated performance of hybrid collector with 2 strips of InGaP/GaAs cells.

Table 4
Updated component costs.

Component	Cost
Cold Bent Glass Mirrors	$16.12/m^2
Solar Collector Frame	$20.00/m^2
Tracker	$3.74/m^2
Dual Junction InGaP/GaAs Cell	$1.14/cm^2
Single Junction InGaP Cell	$0.95/cm^2
Standard Parabolic Trough Receiver	$27.45/m^2
Thermal Energy Storage (TES)	$16,239/MW
Power Block	$1001/kW

Table 5
Total illumination on strip pairs.

	1st strips	2nd strips	3rd strips	4th strips
$\eta_{0,strip}$	13.45%	13.3%	8.32%	3.98%

Table 6
Thermal absorption.

	Thermal Only	2 Strips	3 Strips	4 Strips
$\eta_{0,thermal,InGaP/GaAs}$	77.51%	61.98%	57.12%	54.97%
$\eta_{0,thermal,InGaP}$	77.51%	66.92%	63.60%	62.15%

equation 8 to determine the increase in efficiency according to Fig. 9. Here A_1 is 5 m and the combined length of a strip pair (A_{strip}) is 0.032 m.

$$C_{x,strip} = \eta_{0,strip}\frac{A1}{A_{strip}} \tag{8}$$

The electric output of each strip ($\eta_{cell,strip}$) is calculated from Eq. (9) based on the amount of incident light and cell efficiency at temperature.

$$\eta_{cell,strip} = \eta_{cell}\eta_{Cx}\ (C_{x,strip}) - \beta\ (T - 25\ ^\circ C) \tag{9}$$

The net efficiency of the CPV subsystem ($\eta_{system,cells}$) is calculated from equation 10 by summing the efficiency of each individual strip.

$$\eta_{system,cells} = \sum_{1}^{n_{strips}} \eta_{0,strip}\eta_{cell,strip} \tag{10}$$

All light absorbed by the solar cells but not converted to electricity is exhausted from the system as waste heat ($\eta_{cell,cooling}$) according to Eq. (11).

$$\eta_{cell,cooling} = \sum_{1}^{n_{strips}} \eta_{abs,strip} - \eta_{system,cells} \tag{11}$$

3.3. Thermal model

The emittance of the selective coating on the absorber is estimated from the top 5 research coatings plotted in Fig. 10 (Selvakumar and Barshilia, 2012). Its variation with temperature performs slightly better than the best available commercial coatings and within the realm of current research coatings. As a result the modelled emittance is representative of improved selective coatings which can be expected in the near future.

The net thermal efficiency of the CSP subsystem ($\eta_{thermal}$) accounts for radiative losses which reduce performance below the optical efficiency at elevated temperatures (Eq. (12)). No convective loss terms are included since the absorber is in an evacuated environment. Here ϵ is the emissivity of the selective coating at temperature, σ is the Stefan-Boltzmann constant (W/m^2-K^4), T_{abs} and T_∞ are the temperatures of thermal absorber and environment (K), and *DNI* is the Direct Normal Irradiance which after integrating the ASTM direct solar spectrum is 900 W/m^2.

$$\eta_{thermal} = \eta_{0,thermal} - \frac{A_3\ \epsilon\ \sigma(T_{abs}^4 - T_\infty^4)}{DNI * A_1} \tag{12}$$

This equation is used to calculate thermal efficiency for temperatures up to 700 °C with an assumed environmental temperature (T_∞) of 25 °C (Figs. 12 and 13).

3.4. System exergy and electric efficiencies

As a hybrid system, we must select a metric by which we can evaluate the combined electric and thermal generation. Cogeneration efficiency has been used in the past, but does not take into account the different qualities of the electric and thermal energies produced. Since the Carnot efficiency limit (Eq. (1)) applies to the conversion of heat into useful work (or electricity), solar-to-exergy efficiencies have been proposed as a more practical measure of hybrid solar power generation systems (Branz et al., 2015). Exergy, which is defined as $Q(1-T_C/T_H)$, is the thermodynamic limit to the amount of useful work that can be extracted from a quantity of heat Q at a temperature T_H. The energy and exergy content of electricity are identical since there is no limit to the amount of electricity which can be converted into useful work. In this way, the solar-to-exergy efficiency calculated in Eq. (13) is the maximum possible efficiency of the hybrid system at converting the incoming solar energy into useful work. For these calculations the cold reservoir temperature of the Carnot cycle T_C is assumed to be 37 °C and T_H is the operating temperature of the thermal subsystem.

Table 7
Performance results summary.

	$\eta_{thermal}$ @ 600 °C	$\eta_{system,cells}$	η_{exergy} @ 600 °C	$\eta_{electric}$ @ 600 °C
Dual Junction Solar Cells – 4 Strips	45.9%	9.1%	38.9%	23.7%
Dual Junction Solar Cells – 3 Strips	47.9%	8.2%	39.3%	23.5%
Dual Junctions Solar Cells– 2 Strips	52.5%	6.2%	40.4%	23.0%
Single Junction Solar Cells – 4 Strips	52.6%	5.8%	40.1%	22.6%
Single Junction Solar Cells – 3 Strips	54.0%	5.2%	40.4%	22.5%
Single Junction Solar Cells – 2 Strips	57.1%	4.0%	41.2%	22.3%
Thermal Only	67.1%	0.0%	43.8%	21.5%

Table 8
Hybrid PVT collector cost.

Solar Field Cost	PV/T collector with single Junction InGaP solar cells	PV/T collector with Dual Junction InGaP/GaAs solar cells	Thermal Only Collector
4 Strips of solar cells	$420.52/m^2	$469.16/m^2	$177.32/m^2
3 Strips of solar cells	$359.72/m^2	$396.20/m^2	
2 Strips of solar cells	$298.92/m^2	$323.24/m^2	
	Single Junction	Dual Junction	Thermal Only
$/Watt Exergy			
4 Strips of solar cells	$1.05/$W_{exergy}$	$1.21/$W_{exergy}$	$0.40/$W_{exergy}$
3 Strips of solar cells	$0.89/$W_{exergy}$	$1.01/$W_{exergy}$	
2 Strips of solar cells	$0.73/$W_{exergy}$	$0.80/$W_{exergy}$	
$/Watt Electricity			
4 Strips of solar cells	$1.86/$W_e$	$1.98/$W_e$	$0.82/$W_e$
3 Strips of solar cells	$1.60/$W_e$	$1.69/$W_e$	
2 Strips of solar cells	$1.34/$W_e$	$1.41/$W_e$	

Table 9
Full system cost.

	Single Junction	Dual Junction	Thermal Only
$/Watt Exergy			
4 Strips	$1.91/$W_{exergy}$	$1.98/$W_{exergy}$	$1.42/$W_{exergy}$
3 Strips	$1.77/$W_{exergy}$	$1.81/$W_{exergy}$	
2 Strips	$1.63/$W_{exergy}$	$1.65/$W_{exergy}$	
$/Watt Electricity			
4 Strips	$2.62/$W_e$	$2.61/$W_e$	$1.84/$W_e$
3 Strips	$2.38/$W_e$	$2.35/$W_e$	
2 Strips	$2.17/$W_e$	$2.15/$W_e$	

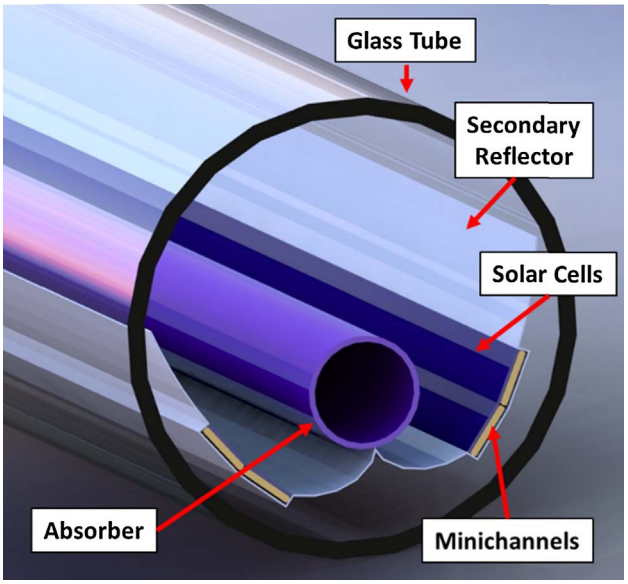

Fig. 14. Rendering of final down-selected hybrid HCE design with 2 mirrored strips of dual junction InGaP/GaAs solar cells integrated into the secondary reflector.

$$\eta_{exergy} = \frac{W_{system,cells} + Q_{thermal}(1-T_C/T_H)}{Q_{solar}} = \eta_{system,cells} + \eta_{Carnot} \cdot \eta_{thermal} \tag{13}$$

In practice, inverter losses will reduce the CPV subsystem electric output during DC-to-AC conversion, and additional plant, power block, and generator losses will reduce conversion of the CSP subsystem into electricity. To account for these, a more realistic solar-to-electric efficiency of the system ($\eta_{electric}$) is calculated with Eq. (14). A 2/3 term is included since actual power block turbines typically reach only ~66% of the Carnot efficiency. Two additional losses are considered to account for plant thermal, storage, and heat exchange losses ($\eta_{HX} = 0.9$), and for parasitic losses ($\eta_{PB,net} = 0.9$).

$$\eta_{electric} = \eta_{system,cells} + \frac{2}{3}\eta_{Carnot}\eta_{thermal}\eta_{HX}\eta_{PB,net} \tag{14}$$

3.5. Economic analysis

System cost is estimated using the costs already listed in NREL's parabolic trough System Advisor Model (SAM). The costs which are modified or added are listed in Table 4. Solar field costs were updated to include the current cost of cold-bent glass-silver mirrors, structural components, and trackers. The hybrid receiver cost was based on the current production cost of parabolic trough receivers with the additional cost of the solar cells. Power block and thermal energy storage (TES) costs were based on estimates of a 100 MW plant using a powder-based HTF and handling system (Cygan, 2016).

4. Results and discussion

4.1. Performance results

84.5% of light is incident on the secondary aperture after shading, primary reflection, and transmission losses. The fraction of light incident on each pair of cell strips ($\eta_{0,strip}$) in Fig. 11 is presented in Table 5 and shows an illumination pattern that validates previous ray

tracing where the 1st and 2nd strips intercept more light than the 3rd and 4th strips.

The fraction of light absorbed by the thermal absorber ($\eta_{0,thermal}$) for each scenario (Table 6) increases with the use of fewer or single rather than dual-junction cells since more light is reflected.

The thermal and full system performance models were evaluated up to operating temperatures of 700 °C and the results for all configurations at 600 °C are listed in Table 7.

4.2. Cost-Performance metrics

The cost metrics in Table 8 are the result of the performance models at 600 °C and the estimated collector costs. From this we see the hybrid converter reaches < $\$1/W_{exergy}$ for the 2 strip hybrid and thermal only configurations.

Full system costs in Table 9 include the thermal energy storage (TES) and power block costs, which were sized relative to the thermal fraction in each scenario.

4.3. Discussion and down-selection

The results presented in this analysis are based on the simulation of a complex system and include many assumptions and simplifications. From a static point of view the current cost of pure thermal-only CSP has a lower dollar per watt electric despite the fact that the hybrid system, by utilizing the high in-band efficiency of the PV component (Fig. 6), has greater net conversion efficiency. Once the cost of III–V cells reaches the SunShot target (Woodhouse and Goodrich, 2013), however, such a system will be economically competitive with pure CSP.

The ultimate difference in full system cost between two strips of single junction or dual junction of $\$0.02/W_e$ is considered negligible and since the dual junction cells provide greater total power output per square meter, the two-strip configuration is selected as the optimal design. The various efficiencies for the thermal-only and hybrid collectors are presented in Figs. 12 and 13, respectively. The solid black lines indicate shading and optical losses, with the net thermal efficiency shown in red and the exergy efficiency in blue. Also drawn in these plots are the net system efficiencies assuming the 2/3 Carnot power block used in this model (dashed black), steam Rankine (cyan), and CO_2 recombination Brayton (magenta) power blocks (Dunham and Iverson, 2014). The balance between increasing Carnot efficiency and increasing heat loss at higher temperatures yields optimal thermal operating temperatures between 500 and 600 °C. A rendering of the final hybrid HCE is shown in Fig. 14.

5. Conclusion and future work

A novel two-stage trough concentrator is designed, simulated, and optimized for the purpose of power generation. Optimization of the secondary CPC concentrator recovers geometric efficiency despite incorporation of flat solar cell strips into a non-continuous profile. 50X geometric concentration is realized on the thermal absorber. Optical, thermal, and cell simulations demonstrated an increase in efficiency and reduction in $\$/W_{exergy}$ as the number of solar cell strips were reduced from four to two. The two strip configuration using dual junction InGaP/GaAs cells was down-selected as the optimal design. It achieves 40% solar-to-exergy and 23% solar-to-electric efficiency at 600 °C with a thermal fraction of 73% and an estimated install cost of $\$2.15/W_e$. At the writing of this manuscript both thermal and hybrid prototypes are being constructed along with a platform for testing up to 650 °C using a particulate HTF.

Acknowledgement

This work was performed with financial support from the Advanced Research Projects Agency - Energy (ARPA-E) under grant ARPA-E DE-AR0000464 awarded by the US Department of Energy (DOE).

References

Advanced Research Projects Agency – Energy and US Department of Energy, 2014. FOCUS Program Overview. < https://arpa-e.energy.gov/?q=arpa-e-programs/focus > .

Behar, O., Khellaf, A., Mohammedi, K., 2013. A review of studies on central receiver solar thermal power plants. Renew. Sustain. Energy Rev. 23, 12–39.

Bendt, P., Rabl, A., Gaul, H.W., Reed, K.A., 1979. Optical analysis and optimization of line focus solar collectors (No. SERI/TR-34-092). Solar Energy Research Inst., Golden, CO (USA).

Branz, H., Regan, W., Gerst, K., Borak, J., 2015. Hybrid solar converters for maximum exergy and inexpensive dispatchable electricity. Energy.

Collares-Pereira, M., Gordon, J., Rabl, A., Winston, R., 1991. High concentration two-stage optics for parabolic trough solar collectors with tubular absorber and large rim angle. Sol. Energy.

Cooper, T., Ambrosetti, G., Malnati, F., Pedretti, A., Steinfeld, A., 2016. Experimental demonstration of high-concentration photovoltaics on a parabolic trough using tracking secondary optics. Prog. Photovolt. Res. Appl. 24 (11), 1410–1426.

Cygan, D., et al., 2016. Full spectrum solar system: hybrid concentrated photovoltaic/concentrated solar power (CPV-CSP). MRS Adv. 1 (43), 2941–2946.

DeJarnette, D., Otanicar, T., Brekke, N., Hari, P., Roberts, K., 2015. Selective spectral filtration with nanoparticles for concentrating solar collectors. J. Photon. Energy 5 (1), 57008.

DeJarnette, D., Tunkara, E., Brekke, N., Otanicar, T., 2016. Nanoparticle enhanced spectral filtration of insolation from trough concentrators. Sol. Energy Mater.

Denholm, P., Wan, Y., Hummon, M., Mehos, M., 2013. Analysis of concentrating solar powerb with thermal energy storage in a California 33% Renewable. Scenario 2013. NREL/TP-6A20-58186.

Dunham, M.T., Iverson, B.D., 2014. High-efficiency thermodynamic power cycles for concentrated solar power systems. Renew. Sustain. Energy Rev. 30, 758–770.

Duquette, B., Otanicar, T., 2012. Comparative economic analysis of concentrating solar technologies. J. Sol. Energy Eng. 135, 024504.

Fernández-García, A., Zarza, E., Valenzuela, L., Pérez, M., 2010. Parabolic-trough solar collectors and their applications. Renew. Sustain. Energy Rev. 14 (7), 1695–1721.

Fu, R., Chung, D., Lowder, T., Feldman, D., Ardani, K., Margolis, R., 2016. NREL U.S. solar photovoltaic system cost benchmark Q1 2016 Report 2016. http://dx.doi.org/10.7799/1325002.

Green, M.A., et al., 2017. Solar cell efficiency tables (version 49). Prog. Photovoltaics Res. Appl. 25 (1), 3–13.

Imenes, A.G., Mills, D.R., 2004. Spectral beam splitting technology for increased conversion efficiency in solar concentrating systems: a review. Sol. Energy Mater. Sol. Cells 84 (1), 19–69.

Ju, X., Xu, C., Han, X., Du, X., Wei, G., Yang, Y., 2017. A review of the concentrated photovoltaic/thermal (CPVT) hybrid solar systems based on the spectral beam splitting technology. Appl. Energy 187 (February), 534–563.

Liu, Y., Hu, P., Zhang, Q., Chen, Z., 2014. Thermodynamic and optical analysis for a CPV/T hybrid system with beam splitter and fully tracked linear Fresnel reflector concentrator utilizing sloped panels. Sol. Energy.

Mehos, M., Turchi, C., Jorgenson, J., Denholm, P., Ho, C., 2016. On the path to sunshot. Advancing Concentrating Solar Power Technology, Performance, and Dispatchability. doi: NREL/TP-5500-65688.

Mehos, M., Turchi, C., Vidal, J., Wagner, M., Ma, Z., Ho, C., Kolb, W., Andraka, C. and Kruizenga, A., 2017. Concentrating Solar Power Gen3 Demonstration Roadmap (No. NREL/TP-5500-67464). NREL (National Renewable Energy Laboratory (NREL), Golden, CO (United States)).

Mojiri, A., Taylor, R., Thomsen, E., Rosengarten, G., 2013. Spectral beam splitting for efficient conversion of solar energy – a review. Renew. Sustain. Energy Rev. 28 (December), 654–663.

NREL SAM Parabolic Trough Model. < https://sam.nrel.gov/ > .

Orosz, M., Zweibaum, N., Lance, T., Ruiz, M., Morad, R., 2016. Spectrum-splitting hybrid CSP-CPV solar energy system with standalone and parabolic trough plant retrofit applications. AIP Conf. Proc. 1734, 70023.

Orosz, M., Zweibaum, N., Lance, T., Ruiz, M., Morad, R., 2016, Spectrum-Splitting hybrid CSP-CPV solar energy system with standalone and parabolic trough plant retrofit applications. In: AIP Conference Proceedings (vol. 1734, issue no. 1, p. 070023). AIP Publishing.

Otanicar, T., DeJarnette, D., Brekke, N., Tunkara, E., 2016. Full spectrum collection of concentrated solar energy using PV coupled with selective filtration utilizing nanoparticles. MRS.

Palmintier, B., Broderick, R., Mather, B., Coddington, M., 2016. On the path to sunshot. Emerging Issues and Challenges in Integrating Solar with the Distribution System 2016. NREL/TP-5D00-65331.

Price, H., Lupfert, E., Kearney, D., Zarza, E., Cohen, G., Gee, R., Mahoney, R., 2002. Advances in parabolic trough solar power technology. J. Sol. Energy Eng. 124 (2), 109–125.

Raush, J.R., Chambers, T.L., 2014. Initial field testing of concentrating solar photovoltaic (CSPV) thermal hybrid solar energy generator utilizing large aperture parabolic trough and spectrum selective mirrors. Int. J. Sustain. Green Energy 3 (6), 123–131.

Schmitz, M., Cooper, T., Ambrosetti, G., Steinfeld, A., 2015. Two-stage solar concentrators based on parabolic troughs: asymmetric versus symmetric designs. Appl. Opt.

Segal, A., Epstein, M., Yogev, A., 2004. Hybrid concentrated photovoltaic and thermal power conversion at different spectral bands. Sol. Energy 76, 591–601.
Selvakumar, N., Barshilia, H., 2012. Review of physical vapor deposited (PVD) spectrally selective coatings for mid-and high-temperature solar thermal applications. Sol. Energy Mater. Sol. Cells.
Shockley, W., Queisser, H.J., 1961. Detailed balance limit of efficiency of p-n junction solar cells. J. Appl. Phys. 32 (3), 510–519.
Shou, C., Luo, Z., Wang, T., Shen, W., Rosengarten, G., Wang, C., et al., 2011. A dielectric multilayer filter for combining photovoltaics with a Stirling engine for improvement of the efficiency of solar electricity generation. Chin. Phys. Lett. 28, 8402.
Smith, D.D., Cousins, P.J., Masad, A., Westerberg, S., Defensor, M., Ilaw, R., Dennis, T., Daquin, R., Bergstrom, N., Leygo, A., Zhu, X., 2013. SunPower's Maxeon Gen III solar cell: high efficiency and energy yield. In: IEEE 39th Photovoltaic Specialists Conference (PVSC), IEEE, 2013, pp. 0908–0913.
Stanley, C., Mojiri, A., Rahat, M., Blakers, A., Rosengarten, G., 2016. Performance testing of a spectral beam splitting hybrid PVT solar receiver for linear concentrators. Appl. Energy 168, 303–313.
Vignarooban, K., Xu, X., Arvay, A., Hsu, K., Kannan, A.M., 2015. Heat transfer fluids for concentrating solar power systems–a review. Appl. Energy 146, 383–396.
Widyolar, B., Jiang, L., Winston, R., 2017. Thermodynamics and the segmented compound parabolic concentrator. J. Photon. Energy 7 (2).
Widyolar, B., Jiang, L., Winston, R., 2018. Spectral beam splitting in hybrid PV/T parabolic trough systems for power generation. Appl. Energy 209, 236–250.
Winston, R., 1970. Light collection within the framework of geometrical optics. JOSA.
Woodhouse, M., Goodrich, A., 2013. A manufacturing cost analysis relevant to single-and dual-junction photovoltaic cells fabricated with III–Vs and III–Vs grown on Czochralski silicon (No. NREL/PR-6A20-60126). National Renewable Energy Laboratory.
Xu, Q., Ji, Y., Riggs, B., Ollanik, A., Farrar-Foley, N., Ermer, J.H., Romanin, V., Lynn, P., Codd, D., Escarra, M.D., 2016. A transmissive, spectrum-splitting concentrating photovoltaic module for hybrid photovoltaic-solar thermal energy conversion. Sol. Energy 137, 585–593.
Yu, Z.J., Fisher, K.C., Wheelwright, B.M., Angel, R.P., Holman, Z.C., 2015. PVMirror: a new concept for tandem solar cells and hybrid solar converters. IEEE J. Photovolt. 5 (6), 1791–1799.